Proceedings of the XIII International Conference "Ion Implantation and Other Applications of Ions and Electrons"

Molecular Dynamics Simulations of Primary Radiation Damage in Silicon Carbide

E. Kucal[a,*], K. Czerski[b,c] and Z. Kozioł[a]

[a] *National Centre for Nuclear Research, Andrzeja Sołtana 7, 05-400 Otwock-Świerk, Poland*
[b] *Institut für Festkörper-Kernphysik gGmbH, Leistikowstraße 2, 14050 Berlin, Germany*
[c] *Institute of Physics, University of Szczecin, Wielkopolska 15, 70-451 Szczecin, Poland*

Doi: 10.12693/APhysPolA.142.747 *e-mail: ewelina.kucal@ncbj.gov.pl

Molecular dynamics simulations provide information on atomic displacement cascades due to the ionic collisions on the time scale of picoseconds and simultaneously account for the effects of crystal structure and temperature. Thus, molecular dynamics can help to understand the specific material behaviour during ion irradiation and make predictions for long-term neutron exposure as well. The latter is especially important for new generations of high-temperature reactors which use ceramics as construction materials. The paper presents the preliminary molecular dynamics simulations of argon irradiation of the SiC sample at very low energies, where mainly elastic collisions dominate, and two different sample temperatures are presented. The obtained results clearly illustrate the time-dependent reduction of the crystal defect number and the influence of the electronic stopping power. Additionally, the number of sustainable crystal defects depends largely on the sample temperature.

topics: silicon carbide, molecular dynamics (MD), irradiation, electronic stopping

1. Introduction

Silicon carbide (SiC) is a promising material for several applications, such as nuclear, electronic, and space ones [1–3]. SiC is an irradiation-resistant material that shows mechanical strength and thermal stability even at high temperatures [4]. Thus, SiC is considered a suitable material for the new concept of nuclear reactors, such as the Dual Fluid Reactor [5, 6]. Its operation temperature will be of the order of 1000°C, and both coolant and fuel are liquid metals. Thus, characterizing and understanding radiation effects, damage creation, and high-temperature repair mechanisms are important for the application of new materials in nuclear reactor technologies. However, the study of crystal defects and related weakening of mechanical features of construction materials resulting from the large neutron flux is very costly and time-consuming. Here, however, ions can be used as a surrogate for neutrons to reduce irradiation time. The same amount of displacement per atom (dpa) can be reached within days instead of decades [7, 8]. Therefore, a full understanding of the difference between neutron and ion irradiation damages is crucial. In the paper, the preliminary results of the modelling of crystal lattice defects induced by low-energy argon ions in the SiC samples are presented.

When the ion passes into the matter, it loses its energy by the elastic collision (nuclear losses — Sn) and by the inelastic collisions (electronic losses — Se). In the low-energy regimes, elastic collisions, which are similar to those induced by neutrons, are dominant, and electronic stopping can be neglected in many cases. For higher energy of ions, inelastic collisions play the most important role in defect production. Electronic energy can be transferred to the lattice and influence the defects dynamics in the material by three mechanisms: Coulomb explosion, lattice relaxation, and the electronic thermal spike [9]. The previous studies on ion irradiation of SiC presented that the energy transferred to the electron system can lead to the annealing of defects [10]. Thus, the molecular dynamics methods will be applied. The electronic stopping effects are investigated only as a reduction of incident ion energy. Transfer of the electronic energy to the lattice is neglected. The previous molecular dynamics simulations of cascades in SiC show that even in low-energy regimes, electronics stopping affects the number of defects [11].

2. Simulation methods

2.1. Molecular dynamics setup

Simulations were performed using the LAMMPS (Large-scale Atomic/Molecular Massively Parallel Simulator) code [12]. This is the classical molecular dynamics simulation code, which computes Newton's equation of motion for the particle system, i.e.,

$$m_i \frac{\partial \boldsymbol{v_i}}{\partial t} = \boldsymbol{F_i}(t), \tag{1}$$

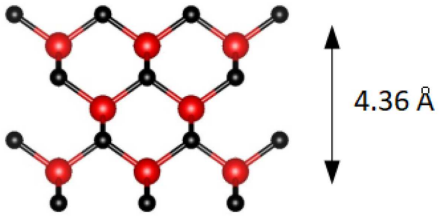

Fig. 1. Stacking sequence of 3C–SiC.

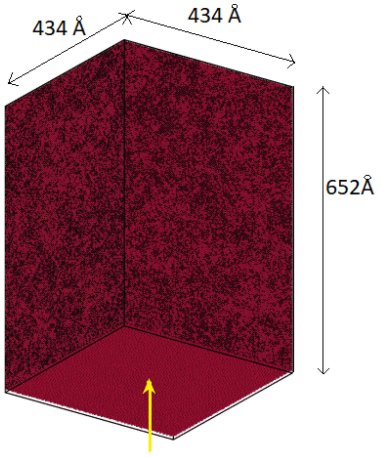

Fig. 2. Schematic figure of the irradiation model. The yellow arrow represents the movement of the Ar ion.

where m_i and $\boldsymbol{v}_i$ are, respectively, the mass and the velocity of the atom i, t is the time step, and $\boldsymbol{F}_i$ is the force acting on the atom i at the time t.

The Geo–Weber interatomic potential [13] was used for the interactions between Si and C atoms in the SiC sample. For the interactions between Ar ions with SiC, the Ziegler–Biersack–Littmark (ZBL) repulsive potential [14] was employed. The SiC sample was generated by Atomsk [15] using the SiC data [16] from the COD database (Crystallography Open Database) [17]. The cubic silicon carbide (Fig. 1) sample had a size of $434 \times 434 \times 652$ Å^3 and contained 12000000 atoms (Fig. 2).

Before irradiation, the samples were equilibrated in the isothermal–isobaric ensemble (NPT) at 300 K or 600 K for 50 ps using the 1 fs timestep. Irradiations were performed in the microcanonical ensemble (NVE) using the variable timestep, automatically selected so that no atom moves further than 0.08 Å. The maximum timestep was 1 fs. The simulations were performed with and without electron stopping.

The defects analysis was made in the 'Open Visualization Tool' (OVITO) by means of the Wigner Seitz analysis [18].

2.2. Electronic stopping power

To simulate the electronic stopping effects, the additional force was added to Newton's equation of motion to reduce the ion velocity [19], giving

$$m_i \frac{\partial \boldsymbol{v}_i}{\partial t} = \boldsymbol{F}_i(t) - \frac{\boldsymbol{v}_i}{|\boldsymbol{v_i}|} S_e, \tag{2}$$

where S_e is the electronic stopping power of the ion.

The electronic stopping power of the incident ions was determined by using the Stopping and Range of Ions in Matter (SRIM) code (see Fig. 3) [14]. In the calculations, the density of SiC equal to 3.16 g/cm^3 was used. SRIM calculate the electronic stopping power for heavy ions based on the Brandt–Kitagawa model, and for low-energy ions, electronic stopping power is proportional to velocity V^a [14].

3. Results and discussion

First, the collision cascade induced by 5 keV Ar ion was analysed. When the ion velocity is reduced not only by the elastic collision but also by the electron stopping, the depth reached by the ion

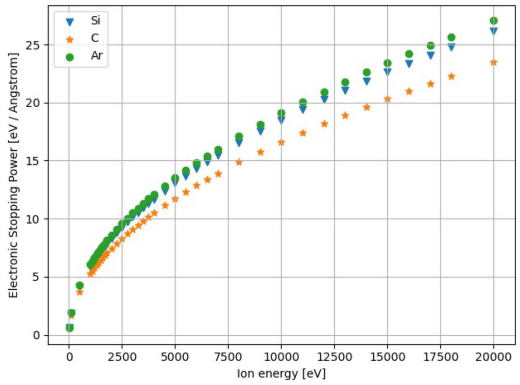

Fig. 3. SRIM calculations of the electronic stopping power of Ar, Si, and C ions in SiC.

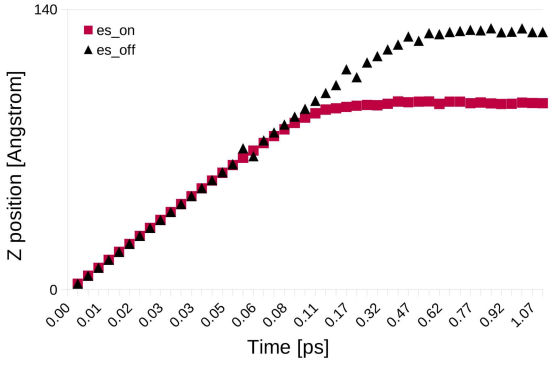

Fig. 4. Position (stopping depth) of Ar ions in the SiC sample (black triangles — without electronic stopping, red rectangles — with electronic stopping).

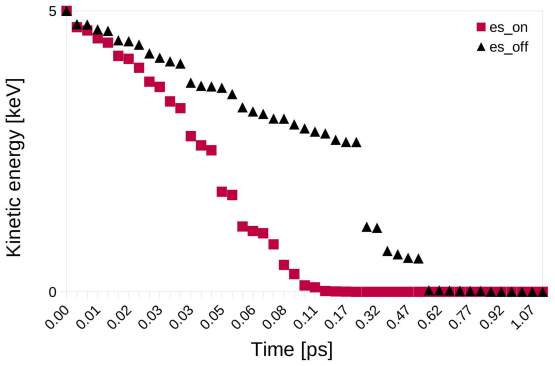

Fig. 5. Kinetic energy loss with time of Ar ions (black triangles — without electronic stopping, red rectangles — with electronic stopping).

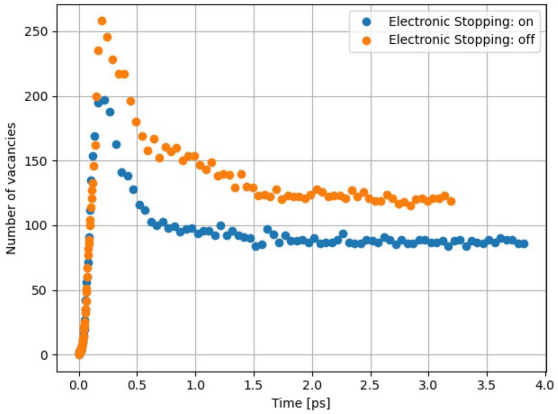

Fig. 6. Number of vacancies produced during the 5 keV Ar cascades at 300 K.

is smaller than in the case when only nuclear stopping is considered (Fig. 4). Obviously, the reduction of kinetic energy is slower in the case when no electron stopping is included (Fig. 5). Figures 4 and 5 present the results for the single ion passage. The reason for the stair-like shape of the kinetic energy loss curve is the different distance between the subsequent collision and the different energy that can be lost during each collision. In the same time step, energy loss can be different as there can be a different number of collisions, and the energy loss can vary during each collision.

Figure 6 shows the number of vacancies calculated by the Wigner–Seitz analysis for the molecular dynamics (MD) simulations with electron stopping (blue line) and without electron stopping (yellow line) for the 5 keV Ar ion cascade at 300 K. The addition of the electronic stopping power results in a fewer number of defects. Importantly, a peak in the number of defects can be observed during the ion penetration. This is followed by a reduction in the number of defects over time until an equilibrium state is reached.

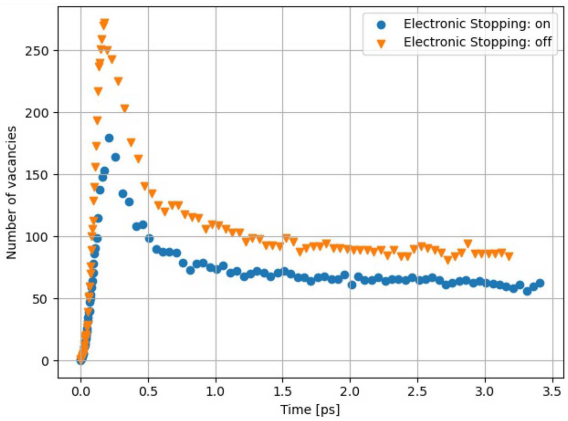

Fig. 7. Number of vacancies produced during the 5 keV Ar cascades at 600 K.

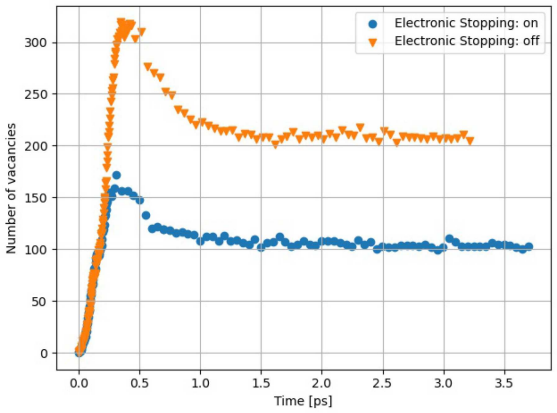

Fig. 8. Number of vacancies produced during the 10 keV Ar cascades.

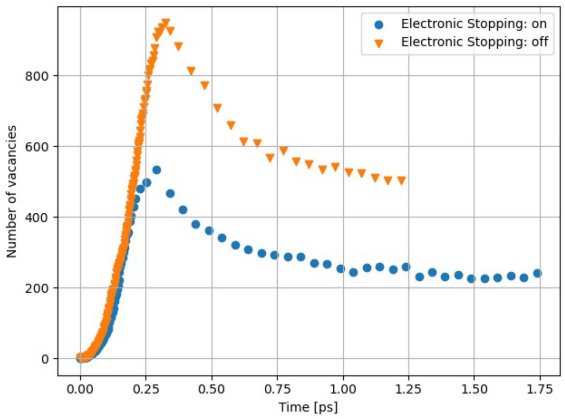

Fig. 9. Number of vacancies produced during the 20 keV Ar cascades.

As follows from Fig. 7, the number of defects is smaller for the cascades observed at 600 K than at 300 K.

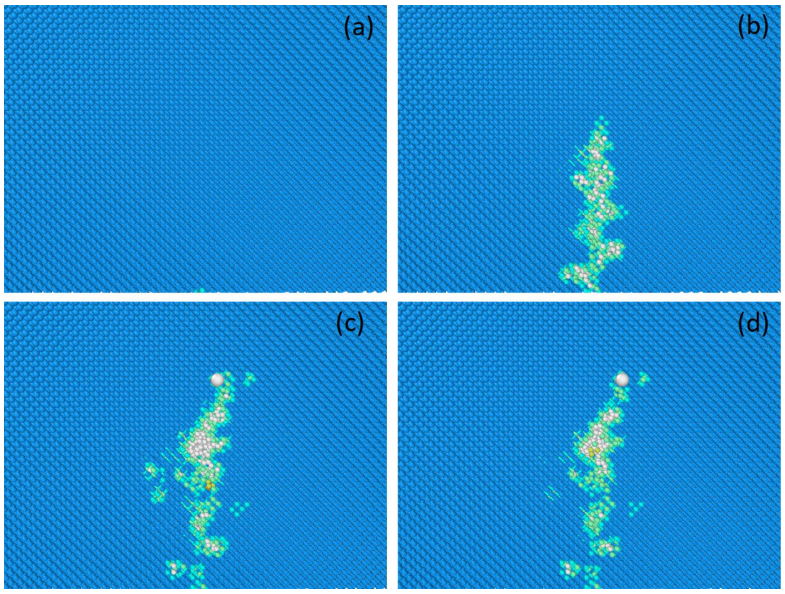

Fig. 10. SiC structure damage at time: (a) 0 ps, (b) 0.07 ps, (c) 0.8 ps, (d) 3.8 ps (simulations with electronic stopping).

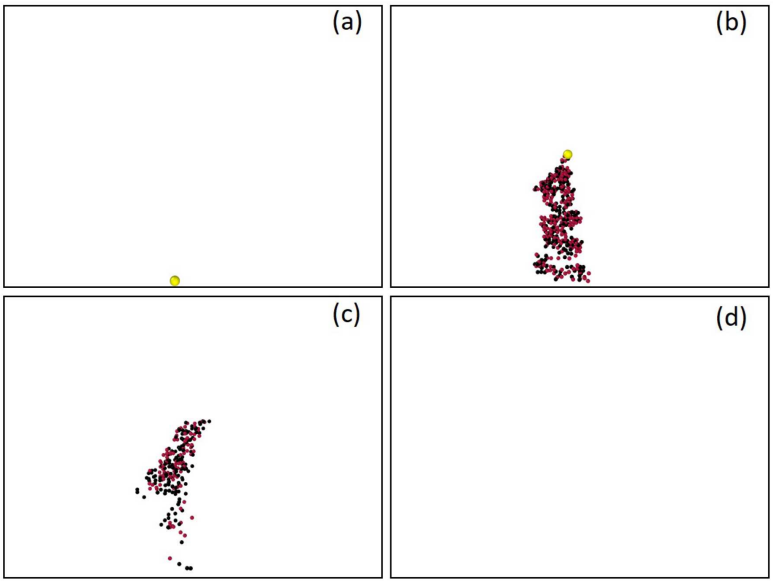

Fig. 11. Visualisation of kinetic energy. Collision cascade induced by 5 keV ions at time: (a) 0 ps, (b) 0.07 ps, (c) 0.8 ps, (d) 3.8 ps (simulations with electronic stopping).

The number of vacancies calculated for 10 keV and 20 keV Ar cascades at 300 K are presented in Figs. 8 and 9, respectively. A greater difference in the number of vacancies is noticed as the ion energy increases. The electronic stopping power exerts greater influence on the results with higher ion energies.

The molecular dynamics simulations provide information about the time dependence of atomic displacement. Figure 10 shows the evolutions of damage in the SiC sample during the 5 keV ion irradiation cascade — initially, the sample has a perfect crystal structure that is destroyed during the ion passage. After the ion passage, some atoms come back to their initial position. Thus during the simulations, a peak of a maximum number of defects is observed, and next, an equilibrium in the sample volume is reached with a constant number of defects. Finally, after a few picoseconds, the kinetic energy of atoms is reduced to 0 eV (Fig. 11). The evolutions of damages in SiC are shown for the simulations with (Fig. 10) and without (Fig. 12) electronic stopping. As for the visualization of kinetic energy — Fig. 11 shows the results of simulations

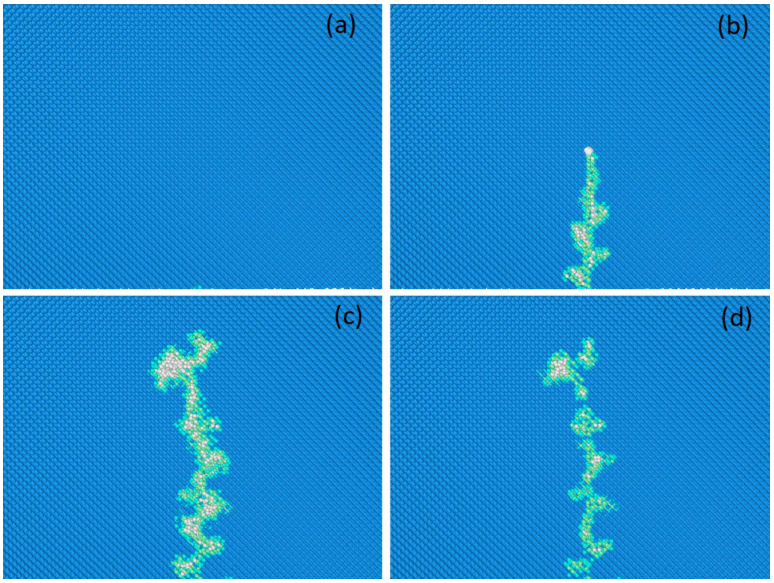

Fig. 12. SiC structure damage at time: (a) 0 ps, (b) 0.06 ps, (c) 0.2 ps, (d) 3.2 ps (simulations without electronic stopping).

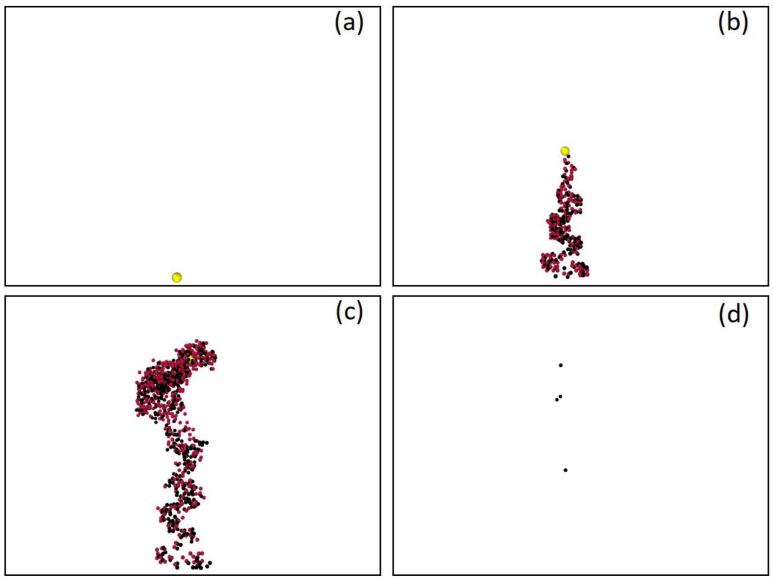

Fig. 13. Visualisation of kinetic energy. Collision cascade induced by 5 keV ions at time: (a) 0 ps, (b) 0.06 ps, (c) 0.2 ps, (d) 3.2 ps (simulations without electronic stopping).

with electron stopping, and Fig. 13 shows the results without electron stopping. Figures 11 and 13 show the atoms with kinetic energy higher than 0.5 eV. The atoms with energy below 0.5 eV were deleted from the sample.

4. Conclusion

In this paper, the advantages of using MD to study the primary radiation damage in SiC are presented. Calculations have been performed for the SiC sample irradiated by the argon ions of energies 5, 10, and 20 keV, for which the nuclear stopping power dominates. MD allows studying the dynamics of the produced crystal defects on the picosecond scale illustrating reduction of originally created defects. This effect depends on both the energy of Ar ions and the temperature of the sample material. The former dependence can be easily explained by the increasing role of the electronic stopping power, although the energy transfer from the electron gas to the SiC lattice was neglected. The latter, however, corresponds to the repair mechanisms of the crystal lattice at higher temperatures. This is

important information for future high-temperature nuclear reactors. However, further investigations of primary radiation damage in SiC are required.

Acknowledgments

The paper was supported by the NCBR project "New Reactor Concepts and Safety Analyses for the Polish Nuclear Energy Program", POWR.03.02.00-00-I005/17 (years 2018-2023).

References

[1] Y. Katoh, L.L. Snead, *J. Nucl. Mater.* **526**, 151849 (2019).

[2] F.F. Wang, Z. Zhang, *CPSS Trans. Power Electron. Appl.* **1**, 13 (2016).

[3] F. Bausier, S. Massetti, F. Tonicello, in: *Proc. 10th European Space Power Conf., Noordwijkerhout 2014*, Ed. L. Ouwehand, Vol. 719, 2014 p. 7.

[4] T. Koyanagi, Y. Katoh, T. Nozawa, *J. Nucl. Mater.* **540**, 152375 (2020).

[5] A. Huke, G. Ruprecht, D. Weißbach, S. Gottlieb A. Hussein K. Czerski, *Ann. Nucl. Energy* **80**, 225 (2015).

[6] J. Sierchuła, M.P. Dąbrowski, K. Czerski, *Prog. Nucl. Energy* **146**, 104126 (2022).

[7] G.S. Was, *J. Mater. Res.* **30**, 1158 (2015).

[8] S.J. Zinkle, L.L. Snead, *Scr. Mater.* **143**, 154 (2018).

[9] G. Schiwietz, K. Czerski, M. Roth, F. Staufenbiel, P. Grande, *Nucl. Instrum. Methods Phys. Res. B* **225**, 4 (2004).

[10] Y. Zhang, R. Sachan, O.H. Pakarinen, M.F. Chisholm, P. Liu, H. Xue, W.J. Weber, *Nat. Commun.* **6**, 8049 (2015).

[11] E. Zarkadoula, G. Samolyuk, Y. Zhang, W.J. Weber, *J. Nucl. Mater.* **540**, 152371 (2020).

[12] A.P. Thompson, H.M. Aktulga R. Berger et al., *Comput. Phys. Commun.* **271**, 108171 (2022).

[13] F. Gao, W.J. Weber, *Nucl. Instrum. Methods Phys. Res. B* **191**, 504 (2002).

[14] J.F. Ziegler, J.P. Biersack, M.D. Ziegler, *SRIM: The Stopping and Range of Ions in Matter*, SRIM, Chester (MD) 2008.

[15] P. Hirel, *Comput. Phys. Commun.* **197**, 212 (2015).

[16] H. Braekken, *Z. Kristallogr. Kristallgeometrie Kristallphys. Kristallchem.* **75**, 572 (1930).

[17] A. Vaitkus, A. Merkys, S. Gražulis, *J. Appl. Crystallogr.* **54**, 661 (2021).

[18] A. Stukowski, *Modelling Simul. Mater. Sci. Eng.* **18**, 015012 (2010).

[19] C.-W. Lee, J.A. Stewart, R. Dingreville, S.M. Foiles, A. Schleife, *Phys. Rev. B* **102**, 024107 (2020).